

# Theoretical investigation of the dynamic electronic response of a quantum dot driven by time-dependent voltage

Xiao Zheng,\* Jinshuang Jin, and YiJing Yan\*

*Department of Chemistry, Hong Kong University of Science and Technology, Kowloon, Hong Kong*

(Dated: submitted on 22 July 2008s)

We present a comprehensive theoretical investigation on the dynamic electronic response of a noninteracting quantum dot system to various forms of time-dependent voltage applied to the single contact lead. Numerical simulations are carried out by implementing a recently developed hierarchical equations of motion formalism [J. Chem. Phys. **128**, 234703 (2008)], which is formally exact for a fermionic system interacting with grand canonical fermionic reservoirs, in the presence of arbitrary time-dependent applied chemical potentials. The dynamical characteristics of the transient transport current evaluated in both linear and nonlinear response regimes are analyzed, and the equivalent classic circuit corresponding to the coupled dot-lead system is also discussed.

PACS numbers: 05.30.-d, 72.10.Bg, 73.63.-b

## I. INTRODUCTION

Motivated by the rapid development in the field of nanoelectronics, a comprehensive and fundamental understanding of quantum transport phenomena has become an urging quest. Theoretical investigations on electronic dynamics of open quantum systems subject to external fields not only provide great insights into relevant physical problems, but also shed light on the design and manipulation of mesoscopic or nanoscopic electronic devices.

Frequency-dependent admittance of mesoscopic systems has been studied by scattering theory<sup>1,2,3</sup> as well as nonequilibrium Green's function (NEGF) method.<sup>4,5,6</sup> At low frequency and low temperature, it was found that to linear order the coherent quantum dynamics of a mesoscopic capacitor can be characterized by a classical circuit in which a resistor and a capacitor are connected in series.<sup>1,2,3,4</sup> The resistor  $R_q$ , often termed as the “charge relaxation resistor”, is related to the time scale for electrons to accumulate on the capacitor in response to external applied voltages, and does not rely on transmission coefficients. For a single-channel, spin-polarized contact with a single lead, it was predicted that at zero temperature  $R_q$  is equal to half a resistance quantum,<sup>1</sup> *i.e.*,

$$R_q = \frac{h}{2e^2} = 12.9k\Omega. \quad (1)$$

The factor 1/2 arises due to the fact that there is only one channel connecting the quantum system to single electrode. This has been confirmed quantitatively by a recent experiment.<sup>7</sup> The capacitance  $C_\mu$ , normally referred to as the “electrochemical capacitance”, was found significantly different from the electrostatic geometric capacitance  $C_0$  due to the limited size of the quantum system and the coherence nature of electron transport. The classical circuit was extended afterwards to include an additional “quantum inductance”  $L_q$ , if one of the capacitor plates is a quantum dot (QD).<sup>5,8,9,10,11</sup>  $L_q$  is of purely quantum origin, and is associated with the time scale of the resonance. For instance, consider a QD consisting of a single spin state and coupled to one electrode. Its dynamic admittance at zero temperature,  $G(\omega)$ , has been expressed analytically by mapping to the equivalent circuit with resistance  $R_q$ , capacitance  $C_\mu$ , and inductance

$L_q$  as<sup>5</sup>

$$G(\omega) = -i\omega C_\mu + \omega^2 C_\mu^2 R_q + i\omega^3 C_\mu^3 R_q^2 - i\omega^3 C_\mu^2 L_q. \quad (2)$$

So far, most work in this field has been conducted within the linear response regime and based on analysis in frequency domain. Keeping in mind that the electron transport is actually a coherent process taking place in real time, it is thus intuitive and straightforward to study the dynamic properties of an open quantum system by probing its transient response to external applied fields. The frequency-dependent admittance  $G(\omega)$  can be obtained via

$$G(\omega) = \frac{I(\omega)}{V(\omega)} = \frac{\mathcal{F}[I(t)]}{\mathcal{F}[V(t)]}, \quad (3)$$

where  $\mathcal{F}$  denotes conventional Fourier transform. It is worth emphasizing here that  $G(\omega)$  is actually independent of the applied voltage  $V(t)$ , so long as its amplitude is kept sufficiently small. Equation (3) shows an alternative route to evaluate  $G(\omega)$  provided that the time-dependent current response  $I(t)$  can be accurately simulated via for example quantum dissipation theory (QDT).

We have recently constructed a formally exact QDT, in terms of hierarchical equations of motion (HEOM), for arbitrary non-Markovian dissipation systems interacting with Gaussian grand canonical ensembles.<sup>12,13,14,15</sup> The theoretical construction was carried out on the basis of the calculus-on-path-integral algorithm, together with the spectral decomposition technique.<sup>14,15,16,17,18</sup> Dynamic responses of the reduced quantum system to external fields can then be obtained through numerical solutions of HEOM for the system density matrix and its associated auxiliary counterparts. For a general many-particle system, the HEOM formalism needs to be properly truncated at a certain finite tier, and the simulated outcomes are considered reliable as long as they are convergent with respect to further inclusion of higher tiers.<sup>12,13,14,15</sup> Great simplification does exist for single-particle systems. It has been proved that for the electron transport through a noninteracting system, the HEOM formalism terminates strictly at the second tier ( $\tilde{n}_{\max} = 2$ ) without approximation.<sup>13</sup>

In this work, we focus on the electron dynamics of a single-level noninteracting QD coupled to an electrode

with finite bandwidth. The paper is organized as follows. In Sec. II, the theoretical framework and practical implementation of the HEOM formalism is introduced. In Appendix, numerical accuracy of the HEOM approach is validated by comparing to exact quantum transport calculations reported in literature. In Sec. III the HEOM approach is applied to simulate the transient electronic dynamics of an open QD. Numerical results in linear-response regime are presented and discussed, along with a detailed analysis of frequency-dependent dynamic admittance. In Sec. IV nonlinear effects are explored. Transient current responses to various types of applied voltages will be exemplified. Conclusions and further comments are given in Sec. V.

## II. METHODOLOGY

The QDT-HEOM formalism developed recently is formally exact for the following standard form of Hamiltonian for quantum transport,<sup>13</sup>

$$H_T = H(t; \{a_{\mu s}, a_{\mu s}^\dagger\}) + \sum_{\alpha} (h_{\alpha} + H'_{\alpha}). \quad (4)$$

The electronic Hamiltonian ( $H$ ) of the system (such as QDs) is rather general, including Coulomb interaction and time-dependent external fields. The electrodes are modeled by noninteracting electrons,

$$h_{\alpha} = \sum_{k \in \alpha} \sum_s \epsilon_{\alpha k s} d_{\alpha k s}^\dagger d_{\alpha k s}. \quad (5)$$

The transfer coupling  $H'_{\alpha}$  between the system and the  $\alpha$ -electrode reads

$$H'_{\alpha} = \sum_{k \in \alpha} \sum_{\mu s} t_{\alpha k \mu s} d_{\alpha k s}^\dagger a_{\mu s} + \text{H.c.} \quad (6)$$

Here,  $a_{\mu s}$  ( $a_{\mu s}^\dagger$ ) is the annihilation (creation) operator associated with the single-electron state  $\mu$  and spin  $s$  of the system,  $d_{\alpha k s}$  ( $d_{\alpha k s}^\dagger$ ) is that associated with the specified  $\alpha$ -electrode single-electron state of energy  $\epsilon_{\alpha k s}$ , and  $t_{\alpha k \mu s}$  is the transfer coupling matrix element. The transfer coupling spectral density functions are

$$J_{\alpha \mu \nu s}(\omega) = 2\pi \sum_{k \in \alpha} t_{\alpha k \mu s}^* t_{\alpha k \nu s} \delta(\omega - \epsilon_{\alpha k s}). \quad (7)$$

In contact of QDT, which describes the dynamics of reduced system density operator  $\rho(t) \equiv \text{tr}_B \rho_T(t)$ , we treat the electrodes as the grand canonical fermionic reservoir bath. We denote  $h_B = \sum_{\alpha} h_{\alpha}$  and the thermodynamic density operator  $\rho_B^{\text{eq}}$  for the bare bath in the absence of time-dependent bias voltage. To describe the stochastic nature of the system-reservoir coupling, consider Eq. (6) in the  $h_B$ -interaction picture,  $H'_{\alpha}(t) = \sum_{\mu s} \hat{f}_{\alpha \mu s}^\dagger(t) a_{\mu s} + \text{H.c.}$ , with (setting  $\hbar = 1$ )

$$\hat{f}_{\alpha \mu s}^\dagger(t) \equiv e^{i h_B t} \left( \sum_{k \in \alpha} t_{\alpha k \mu s} d_{\alpha k s}^\dagger \right) e^{-i h_B t}. \quad (8)$$

These stochastic bath operators satisfy the Gaussian statistics with Wick's theorem for thermodynamic average over the grand canonical fermionic bath ensembles with  $\rho_B^{\text{eq}}$ . The effects of electrodes on the system

are completely the following nonzero reservoir correlation functions,<sup>13</sup>

$$C_{\alpha \mu \nu s}^+(t - \tau) \equiv \langle \hat{f}_{\alpha \mu s}^\dagger(t) \hat{f}_{\alpha \nu s}(\tau) \rangle_B, \quad (9a)$$

$$C_{\alpha \mu \nu s}^-(t - \tau) \equiv \langle \hat{f}_{\alpha \mu s}(t) \hat{f}_{\alpha \nu s}^\dagger(\tau) \rangle_B, \quad (9b)$$

which relate to the spectral density functions (denoting  $J_{\alpha \mu \nu s}^+ \equiv J_{\alpha \mu \nu s}^- \equiv J_{\alpha \mu \nu s}$ ) via<sup>13</sup>

$$C_{\alpha \mu \nu s}^\pm(t - \tau) = \frac{1}{2\pi} \int_{-\infty}^{\infty} d\omega \frac{e^{\pm i\omega(t-\tau)} J_{\alpha \mu \nu s}^\pm(\omega)}{1 + e^{\pm \beta_{\alpha}(\omega - \mu_{\alpha})}}. \quad (10)$$

Here  $\beta_{\alpha} \equiv 1/(k_B T_{\alpha})$  and  $\mu_{\alpha}$  are inverse temperature and equilibrium chemical potential of lead  $\alpha$ , respectively.

In the presence of time-dependent voltage applied to electrodes, the Fermi energy is subject to a homogenous time-dependent shift, *i.e.*,  $\tilde{\mu}_{\alpha}(t) = \mu_{\alpha} + \Delta_{\alpha}(t)$ . The relevant nonequilibrium correlation functions are<sup>13</sup>

$$\tilde{C}_{\alpha \mu \nu s}^\pm(t, \tau) = \exp \left[ \pm i \int_{\tau}^t dt' \Delta_{\alpha}(t') \right] C_{\alpha \mu \nu s}^\pm(t - \tau). \quad (11)$$

From the perspective of QDT, the electronic dynamics of an open system is mainly characterized by  $\rho(t)$  and the transient current through each lead. For linear coupling Hamiltonian of Eq. (6), system-lead dissipative interactions can be exactly captured by the Feynman-Vernon influence functional in path integral.<sup>19</sup> Time derivatives on the influence functional are performed in a hierarchical manner, and thus lead to the construction of a formally exact hierarchical set of coupled EOM for a general non-Markovian dissipative system.<sup>12,13,14,15</sup> The final HEOM is cast into the following compact form (see Ref. 13 for details):

$$\dot{\rho}_{\mathbf{n}} = -[i\mathcal{L} + \gamma_{\mathbf{n}}(t)] \rho_{\mathbf{n}} + \rho_{\mathbf{n}}^{\{-\}} + \rho_{\mathbf{n}}^{\{+\}}, \quad (12)$$

with  $\mathcal{L}\hat{O} \equiv [H(t), \hat{O}]$  for an arbitrary operator  $\hat{O}$ . The basic variables of Eq. (12) are  $\rho(t)$  and associated auxiliary density operators (ADOs)  $\rho_{\mathbf{n}}(t)$ , where  $\mathbf{n}$  is an index set covering all accessible derivatives of the influence functional. With  $C_{\alpha \mu \nu s}^\pm(t)$  expanded by an exponential series via a spectral decomposition technique,<sup>16,17,18</sup>  $\mathbf{n}$  involves an  $\tilde{n}$ -fold combination of  $(\sigma, \alpha, \mu, \nu, s, m)$  that characterize the exponential series expansion with  $\sigma = \pm$ . Therefore,  $\rho_{\mathbf{n}}|_{\tilde{n}=0} \equiv \rho(t)$ , and  $\gamma_{\mathbf{n}}|_{\tilde{n}=0} = \rho_{\mathbf{n}}^{\{-\}}|_{\tilde{n}=0} = 0$ ;  $\rho_{\mathbf{n}}|_{\tilde{n} \neq 0}$  is an ADO at the  $\tilde{n}^{\text{th}}$ -tier;  $\gamma_{\mathbf{n}}(t)$  collects the related exponents along with  $i\Delta_{\alpha}(t)$ , to  $\rho_{\mathbf{n}}$ ; and  $\rho_{\mathbf{n}}^{\{-\}}$  and  $\rho_{\mathbf{n}}^{\{+\}}$  are the nearest lower- and upper-tier counterparts of  $\rho_{\mathbf{n}}$ , respectively. In particular, the 1<sup>st</sup>-tier ADOs,  $\rho_{\mathbf{n}}(t)|_{\tilde{n}=1} = \rho_{\alpha \mu \nu s m}^\sigma(t)$ , determine exclusively the transient current of spin- $s$  through the lead  $\alpha$  as<sup>13</sup>

$$I_{\alpha s}(t) = -2 \text{Im} \sum_{\mu \nu m} \text{tr} [a_{\mu s} \rho_{\alpha \mu \nu s m}^+(t)]. \quad (13)$$

Here the trace is performed for all QD degrees of freedom.

The HEOM formalism has been implemented for a general dissipative system. Details of the programming techniques will be published elsewhere. The accuracy of our numerical approach is verified extensively; see Appendix.

In the following we will focus on a single-level non-interacting QD coupled to one lead, and thus omit the

indexes of  $(\alpha\mu\nu s)$  hereafter. The energy of the spinless QD-level is  $\epsilon_0$ . An external voltage  $V(t)$  is applied to the coupling lead from  $t = 0$ , which excites the QD out of equilibrium. The lead energy level are shifted due to the voltage,  $\Delta(t) = -eV(t)$ , and so is the lead chemical potential  $\mu(t) = \mu + \Delta(t)$ , where  $e$  is the elementary charge and  $\mu$  is the equilibrium lead Fermi energy that is set to zero hereafter, *i.e.*,  $\mu = 0$ . A widely used Drude model is adopted for the spectral density function of the coupling lead,

$$J(\omega) = \frac{\Gamma W^2}{\omega^2 + W^2}. \quad (14)$$

In equilibrium (in absence of voltages) or in a steady state (under a constant external voltage), the rhs of Eq. (12) is equal to zero, and the HEOM reduce to a closed set of linearly coupled equations for  $\{\rho_n(0)\}$ . The subsequent evolution of  $\{\rho_n(t > 0)\}$  is characterized by Eq. (12), with the equilibrium density operators as initial conditions, *i.e.*,  $\rho_n(0) = \rho_n^{\text{eq}}$ . With our current coding, the reduced system is spanned in a Fock-state representation. The linear sparse problem for solving the equilibrium or steady-state  $\rho_n$  is tackled by the biconjugate gradient method,<sup>20</sup> and the time propagation of  $\rho_n(t)$  in follows the 4<sup>th</sup>-order Runge-Kutta algorithm. It has been shown<sup>13</sup> that for an noninteracting system, the HEOM formalism is *exact* with the terminal tier of  $\tilde{n}_{\text{max}} = 2$ .

### III. DYNAMIC ADMITTANCE IN LINEAR RESPONSE REGIME

#### A. Transient electronic dynamics and frequency-dependent admittance

We now apply the HEOM approach to investigate the dynamic admittance of the single-lead QD. It is presumed that the geometric capacitance can be neglected for the QD of interest, *i.e.*,  $C_0 \rightarrow \infty$ , which means that no charging energy is required for an electron to populate the QD level. It is also assumed that the QD level energy  $\tilde{\epsilon}_0(t) = \epsilon_0 + \Delta_D(t)$  does not change with time, *i.e.*,  $\Delta_D(t) = 0$  at any time  $t$ , which is consistent with the  $C_0 \rightarrow \infty$  hypothesis. The dynamic admittance of a single-lead QD is extracted from the real-time current responses  $I(t)$  to external driving voltages  $V(t)$  based on Eq. (3).

The general HEOM formalism admits an arbitrary form for the external voltage  $V(t)$ . Transient currents due to various types of applied *ac* voltages are shown in Fig. 1. The time-dependent voltage adopted for Fig. 1(c) corresponds to  $\Delta(t) = \Delta(1 - e^{-t/\tau_a})$ , where the time constant  $\tau_a > 0$  dominates the switch-on rate of the voltage, and the asymptotic limit  $\tau_a \rightarrow 0^+$  actually describes a step function. In Fig. 1(c)  $\tau_a$  is taken as 50 ps. The driving voltage for Fig. 1(d) is a sinusoidal function:  $\Delta(t) = \Delta[1 - \cos(\omega t)]$  with the period  $(2\pi/\omega) = 40$  ps. In Fig. 1(e) and (f) the open QD system is excited out of equilibrium by a Gaussian voltage pulse as follows,

$$\Delta(t) = \begin{cases} \Delta e^{-(t-\tau_c)^2/\tau_b^2} & 0 \leq t \leq \tau_c \\ \Delta e^{-\kappa(t-\tau_c)^2/\tau_b^2} & t > \tau_c \end{cases}, \quad (15)$$

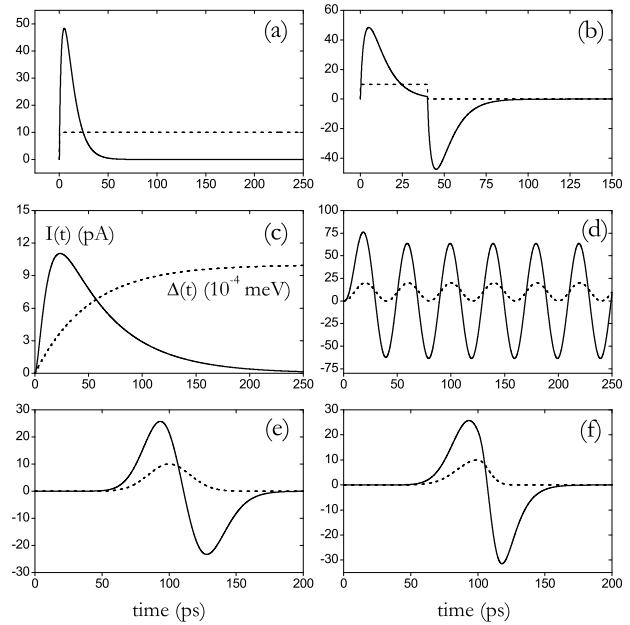


FIG. 1: Transient current responses to various types of external voltages. The solid (dashed) curves represent the time-dependent current  $I(t)$  [energy shift  $\Delta(t) = -eV(t)$ ]. The parameters adopted are as follows (in unit of meV):  $\epsilon_0 = \mu = 0$ ,  $\Gamma = 0.08$ ,  $T = 0.026$  and  $W = 3$ . The switch-on voltages are (a) a step function; (b) a square pulse; (c) an exponential function; (d) a sinusoidal function; (e) a symmetric Gaussian function; and (f) an asymmetric Gaussian function with the same peak amplitude  $\Delta = 0.001$  meV.

where  $\tau_b$  and  $\tau_c$  determine the width and the center of the Gaussian pulse, respectively, and the factor  $\kappa$  controls the asymmetry of the pulse before and after  $\tau_c$ . In Fig. 1(e)  $\tau_b = 22$  ps,  $\tau_c = 100$  ps and  $\kappa = 1$  are employed, *i.e.*, the Gaussian pulse is symmetric in time, while in Fig. 1(f)  $\kappa = 4$  is adopted, which means that  $\Delta(t)$  drops faster than it rises. In the linear response regime, the dynamic admittance of the open QD system obtained by Eq. (3) reflects the intrinsic physical features of the open system, and is thus independent of the specific temporal behavior of  $\Delta(t)$ , as long as its amplitude  $\Delta$  is kept sufficiently low. Among the various time-dependent voltages mentioned above, the asymmetric Gaussian pulse is found to be a convenient candidate for a Fourier analysis, since both  $V(t)$  and the corresponding  $I(t)$  have nonzero values only within a finite time interval. Therefore, subsequent numerical analyses in this section will be based on simulations with asymmetric Gaussian voltage pulses, if no additional remarks are given. The purpose of introducing asymmetry to the Gaussian voltage pulse [see Eq. (15)] is to save computational effort while maintaining the accuracy of the resulting admittance  $G(\omega)$ , especially in the low frequency range (to be elaborated later). Transient current driven by some other types of applied voltages will be discussed in Sec. IV, such as step-function and delta-function voltage pulses.

It is noted that for a voltage pulse consisting of both turn-on and turn-off sides, a sign change is always observed for the response current [*cf.* Fig. 1(b), (e) and (f)], which shows that an entirely positive  $\Delta(t)$  can result in

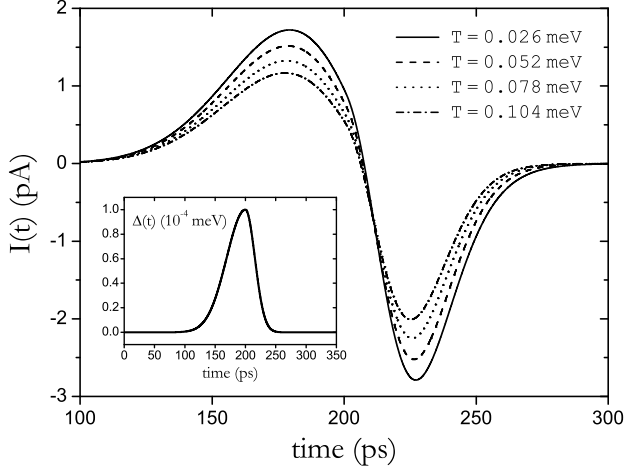


FIG. 2: Transient current responses to an asymmetric Gaussian voltage pulse (see the inset) under various temperatures. The parameters are  $\kappa = 4$ , and the rests in unit of meV:  $\Delta = 10^{-4}$ ,  $\Gamma = 0.1$  and  $W = 10$ .

a negative current. This is actually due to the fact that there is only one lead coupled to the QD. As the voltage is turned on, the lead chemical potential is increased, which drives the electrons flowing from the lead to the QD (positive current) until the voltage reaches its maximum; and then while the voltage decays, the excess electrons residing on the QD gradually wane back to the lead, which reverses the direction of the electron flow (negative current). As the voltage pulse vanishes at  $t \rightarrow \infty$ , the initial equilibrium is restored ultimately. Therefore, during the entire voltage on-off cycle there is no net charge accumulating on the QD. Based on the charge continuity equation, we should have  $I(\omega = 0) = \int_{-\infty}^{\infty} I(t) dt = 0$ , and this equality has been verified for all the cases plotted in Fig. 1, except for (d) where  $\Delta(t \rightarrow \infty) \neq 0$ . For the case of an asymmetric Gaussian voltage, it is intriguing to see the negative peak current (31.5 pA) is larger than the positive counterpart (25.8 pA); see Fig. 1(f). This is ascribed to the non-adiabatic charging effect. In general, the more rapidly the external voltage changes, the larger is the transient response current in terms of its amplitude. Here the turn-off side of voltage possesses a steeper slope ( $\kappa > 1$ ), and hence the electrons going out from the QD at  $t > \tau_c$  is faster than the rate of electron inflow at  $t < \tau_c$ . For the same reason, the peak current under a step function voltage is larger than that under an exponential function voltage; cf. Fig. 1(a) and (c).

In linear-response regime, the dynamic admittance of a noninteracting QD coupled to a single lead has been derived by the NEGF method with the wide-band limit (WBL) approximation.<sup>4,5</sup> Extension to a finite bandwidth case is straightforward. With a Lorentzian spectral density function  $J(\epsilon)$  [cf. Eq. (14)], the linear-response admittance  $G(\omega)$  at any temperature can be evaluated via Eq. (2) for both resonant ( $\epsilon_0 = \mu$ ) and off-resonant ( $\epsilon_0 \neq \mu$ ) cases with  $\mu$  being the equilibrium lead chemical potential.

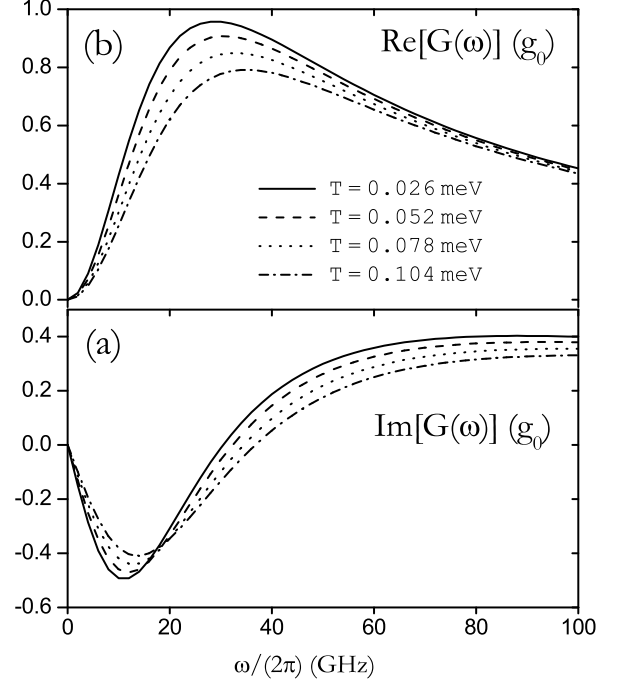


FIG. 3: (a) Real and (b) imaginary parts of frequency-dependent admittance under various temperatures. Same parameters are adopted as in Fig. 2.

### B. Resonant tunneling cases

We first investigate the cases where the dot level  $\epsilon_0$  is in resonance with the Fermi energy of the lead  $\mu$ , i.e.,  $\epsilon_0 = \mu = 0$ . In Fig. 2 we plot the transient currents driven by an asymmetric Gaussian voltage pulse under various temperatures. For all calculations carried out, the amplitude of applied voltage is kept lower than  $10 \mu\text{V}$  throughout the simulation time to ensure the system dynamics remains in the linear response regime. Upon the application of the driving voltage, the QD undergoes a complete period of charge accumulation and depletion, which is synchronized with the on-off cycle of the external bias. It is observed that the current amplitude is suppressed as the temperature rises. The corresponding frequency-dependent admittances are shown in Fig. 3, where the conductance quantum  $g_0 = 2e^2/h = 7.75 \times 10^{-5} \text{ S}$  is used as the unit for  $G(\omega)$ . It is noted that the imaginary part of  $G(\omega)$  changes its sign within the frequency range  $\omega/(2\pi) \in (30, 40) \text{ GHz}$  [see Fig. 3(a)]. This implies that the electronic dynamics of the reduced system exhibits distinct phase features at different frequencies. In the low frequency regime,  $\text{Im}[G(\omega)]$  is almost proportional to  $\omega$ , hence the open QD system resembles much a capacitor. Since the geometric capacitance  $C_0$  is neglected for the open QD system, this capacitor-like behavior is of pure quantum coherence nature, and is thus referred to as electrochemical capacitance  $C_\mu$ . As  $\omega$  increases, the linear relation for  $\text{Im}[G(\omega)]$  breaks down, and the phase shift between the current and voltage diminishes gradually until getting reversed upon the sign change. This agrees with previous studies on the  $C_\mu$  of the same open QD system.<sup>5</sup>

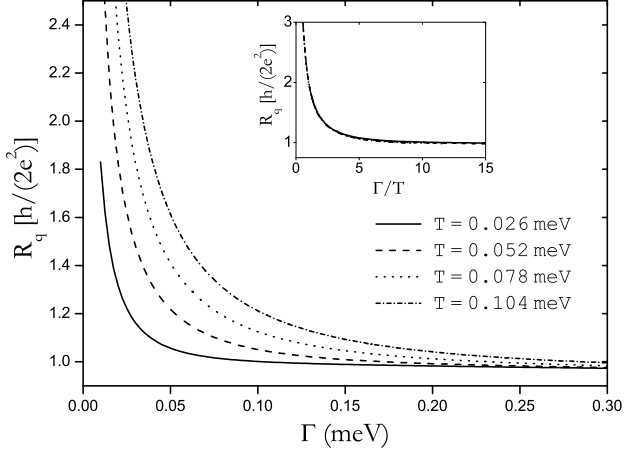


FIG. 4:  $\text{Re}[Z(\omega \rightarrow 0^+)]$  as a function of  $\Gamma$  under various temperatures. Other parameters are (in unit of meV):  $\Delta = 10^{-4}$  and  $W = 10$ . The inset plots  $R_q$  as a function of a dimensionless quantity  $\Gamma/T$ .

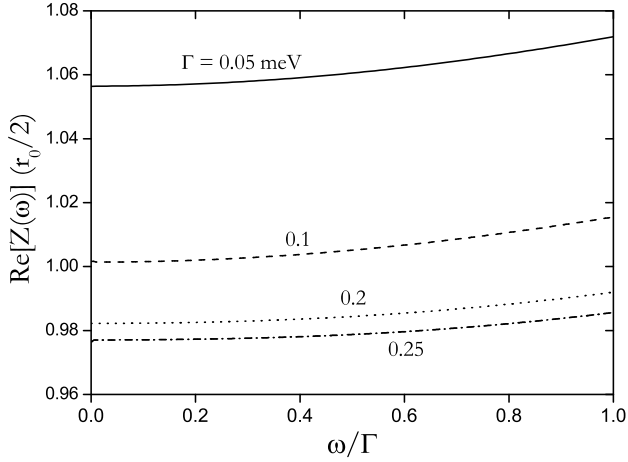


FIG. 5:  $\text{Re}[Z(\omega)]$  as a function of the dimensionless quantity  $\omega/\Gamma$ . The lines represent the different values of  $\Gamma$ . Other parameters are (in unit of meV):  $T = 0.026$  and  $W = 10$ .

At zero temperature, it has been demonstrated that the dynamic admittance of the open QD system can be quantified by a classical  $RLC$  circuit in the low frequency range ( $\omega < \Gamma$ ).<sup>5</sup> Adopting the convention in quantum transport theory, the electrical impedance of the  $RLC$  circuit is expressed as follows [cf. Eq. (2)],

$$Z(\omega) \equiv [G(\omega)]^{-1} = R_q + \frac{1}{-i\omega C_\mu} - i\omega L_q. \quad (16)$$

Although  $Z(\omega)$  diverges at  $\omega = 0$  [due to the fact that  $I(\omega) = 0$  at  $\omega = 0$ ],  $\text{Re}[Z(\omega)] = R_q$  is a finite constant and independent of  $\omega$ , provided that  $\omega \geq 0^+$ . The charge relaxation resistance  $R_q$  is deduced to be  $r_0/2$  [cf. Eq. (1)], where  $r_0 = h/e^2$  is the resistance quantum. At finite temperatures the complex impedance of the open QD system is calculated by the HEOM approach together with Eq. (3). The resulting  $\text{Re}[Z(\omega)]$  at  $\omega \rightarrow 0^+$  are plotted in Fig. 4 as a function of  $\Gamma$ . To ensure the accuracy of  $Z(\omega)$ , it is vital to have high precision for the calculated  $I(\omega)$ , especially in the low  $\omega$  range. This can be achieved

by tactically tuning the driving voltages. For instance, introducing asymmetry to the Gaussian pulse [*i.e.*, setting  $\kappa \neq 1$  in Eq. (15)] magnifies the values of  $I(\omega)$  as  $\omega \rightarrow 0^+$ , and thus reduces its relative errors. However, no matter what type of external voltage is applied, the HEOM approach should yield exactly the same  $G(\omega)$  in linear response regime. This has been proved via extensive tests (see Sec. IV for the results with delta-function voltages).

From Fig. 4 it is revealed that at a finite temperature,  $R_q$  is no longer a universal constant, but depends on the system-bath coupling strength  $\Gamma$ . In particular,  $R_q$  deviates significantly from the “universal” value  $r_0/2$  when  $\Gamma$  is minute. To understand this temperature dependence of charge relaxation resistance, we plot in the inset of Fig. 4 the calculated  $R_q$  as a function of a dimensionless quantity  $\Gamma/T$  under various temperatures. All the curves are found to overlap each other, which indicates a general trend of coherent electronic dynamics. This thus reveals that the response current spectrum depends parametrically on the ratio  $\Gamma/T$ .

As shown in the inset,  $R_q$  becomes drastically larger than  $r_0/2$  as  $\Gamma \ll 5T$ . This can be rationalized as follows. The QD level ( $\epsilon_0 = 0$ ) possesses an intrinsic broadening with the magnitude  $\Gamma$  due to the dissipative interaction with the lead. At zero temperature, all the tunneling electrons are injected along the Fermi surface of the lead ( $\mu = 0$ ), and hence the open QD system is in full resonance resulting in  $R_q = r_0/2$ . At a finite temperature, some electrons in the lead are thermally excited. However, as long as the energies of the excited electrons (or holes) remain in the linewidth of the QD level, *i.e.*,  $(-\Gamma, \Gamma)$ , the electronic dynamic coherence is still conserved. If the temperature is increased further so that a significant portion of thermally excited electrons cannot be covered by the aforementioned energy window associated with the QD level, the resonance is partially lost. Therefore, the mismatch between the energy of tunneling electrons and that of QD level disfavors the electron transport process and gives rise to a much larger  $R_q$ . This is consistent with Fig. 5 where  $\text{Re}[Z(\omega)]$  versus the dimensionless quantity  $\omega/\Gamma$  for different values of  $\Gamma$  are plotted. It is shown that in the low frequency ( $\omega < \Gamma$ ) regime,  $\text{Re}[Z(\omega)]$  is rather insensitive to  $\omega$  (with the maximal deviation of roughly 3% at  $\omega = \Gamma$ ) for all simulated cases. However,  $\text{Re}[Z(\omega)]$  assumes a larger average value as  $\Gamma$  becomes weaker. Therefore, we conclude that at a finite temperature, the charge relaxation resistance  $R_q$  is no longer a universal constant, but depends on both the temperature and the coupling strength  $\Gamma$ .

### C. Off-resonant tunneling cases

We now turn to the cases where  $\epsilon_0 \neq \mu$ . It is important to point out that as  $\epsilon_0$  rises away from  $\mu$ , a much larger number of exponential functions needed to be adopted for the expansion of  $C_{\alpha\mu\nu s}^\pm(t)$  to guarantee the accuracy of the outcomes. It is inferred that the short-memory components of bath correlation functions play significant roles in the off-resonant cases. Figure 6 depicts the transient current responses to an asymmetric Gaussian volt-

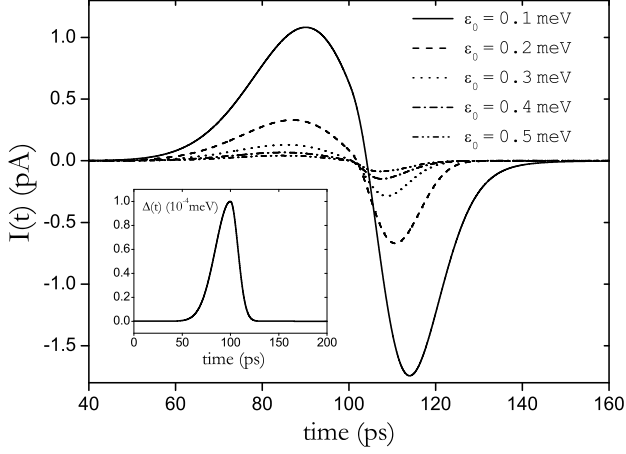


FIG. 6: Transient current responses to an asymmetric Gaussian voltage pulse (see the inset) for various off-resonant cases. The parameters are  $\kappa = 4$ ,  $\tau_c = 100$  ps,  $\tau_b = 22$  ps, and the rests in unit of meV:  $\Delta = 10^{-4}$ ,  $T = 0.104$ ,  $\Gamma = 0.1$  and  $W = 10$ .

age pulse for various dot energies  $\epsilon_0$ . The current profiles are analogous to the resonant cases shown in Fig. 2, except that the peak amplitude of  $I(t)$  declines drastically as  $\epsilon_0$  deviates continually from  $\mu$ . The corresponding frequency-dependent admittances are depicted in Fig. 7, where both the real and imaginary parts of  $G(\omega)$  exhibit conspicuous blue shifts with the increasing  $\epsilon_0$ . Intuitively, as the dot level goes up, fewer electrons can tunnel through the potential barrier at the system-bath interface and dwell on the QD, and hence the electrochemical capacitance of the reduced system becomes smaller. This coincides with the tendency shown in Fig. 7(a), where the descending slope of  $\text{Im}[G(\omega)]$  in the low  $\omega$  range becomes less steep as  $\epsilon_0$  increases.

#### IV. TRANSIENT ELECTRONIC DYNAMICS IN NONLINEAR RESPONSE REGIME

As the applied voltage intensifies, the dynamic response of the open QD system goes beyond the linear response regime. In such a case, the associated frequency-dependent admittance depends explicitly on the specific type of the external voltage. It is thus difficult to derive a general expression for  $G(\omega)$ , and the electronic dynamics needs to be studied case by case.

Since the HEOM approach admits arbitrary time-dependent applied voltages, no extra effort is required for calculations under higher external biases, *i.e.*, the numerical procedures of Eq. (3) can be extended straightforwardly to the nonlinear response regime. In this section, transient currents driven by three types of turn-on voltages will be presented in the subsections: (a) an asymmetric Gaussian function, (b) a step function, and (c) a delta function.

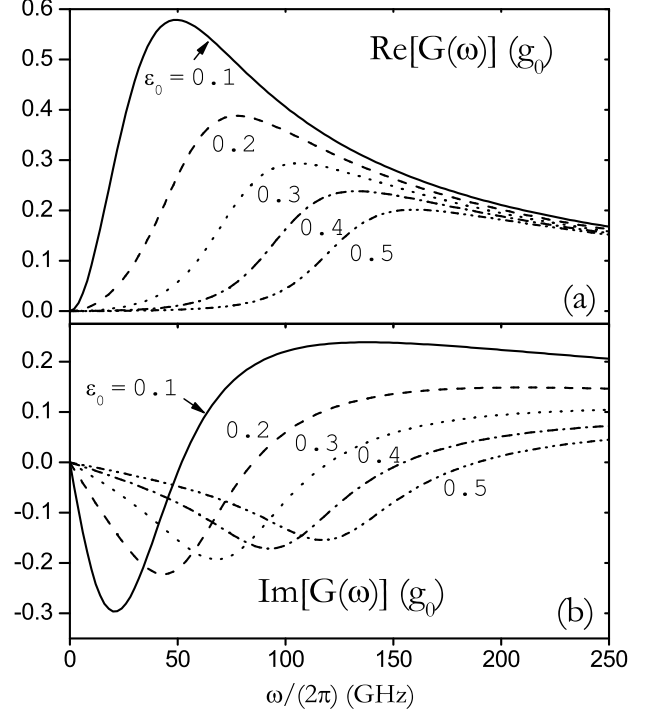


FIG. 7: (a) Real and (b) imaginary parts of  $G(\omega)$  for various off-resonant cases. Same parameters are adopted as in Fig. 6. In both (a) and (b), the lines represent different  $\epsilon_0$  in unit of meV.

##### A. Frequency-dependent admittance under asymmetric Gaussian voltage pulses

In Fig. 8 we plot the transient currents under asymmetric Gaussian voltages of the amplitudes  $\Delta$  ranging from 0.1 to 1 meV (recall that in linear response cases,  $\Delta$  is set lower than  $10^{-4}$  meV). It is observed that as  $\Delta$  increases, the electron accumulation and depletion periods become separated from each other. Especially for  $\Delta = 1$  meV, the transient current almost vanishes in the time interval of 150 ~ 200 ps, whereas in the due course  $\Delta(t)$  still keeps rising. The corresponding frequency-dependent admittances are shown in Fig. 9, where two adjacent lines are separated vertically by  $0.5g_0$  for clarity. It is evidently indicated that as the applied voltage increases, higher-energy current components are gradually activated, and the resulting  $G(\omega)$  appears more fluctuating. The complicated lineshape of  $G(\omega)$  seems to exclude any simple equivalent classical circuit that can describe quantitatively the coherent electronic dynamics of the open QD system.

##### B. Transient current driven by a step function voltage and its spectrum analysis

The exact time-dependent current  $I(t)$  driven by a step function voltage has been obtained by the NEGF method.<sup>21</sup> Especially with the WBL approximation ( $W \rightarrow \infty$ ), its Fourier transform  $I(\omega)$  can be evaluated conveniently via an EOM for the reduced single-electron density matrix for the reduced system.<sup>22</sup> Under a step

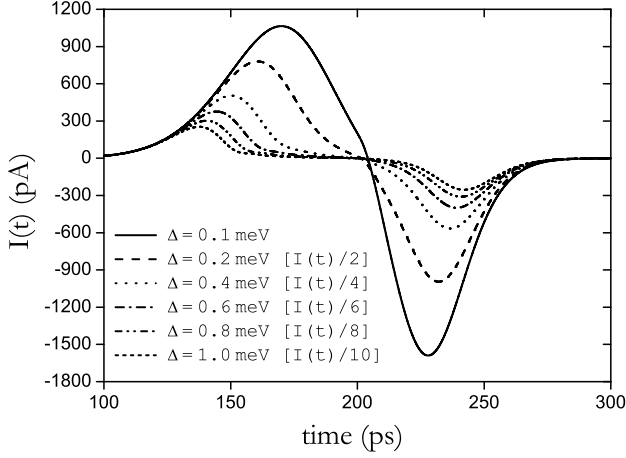


FIG. 8: Scaled transient currents under asymmetric Gaussian voltages of different amplitudes. The parameters are  $\kappa = 4$ ,  $\tau_c = 200$  ps,  $\tau_b = 44$  ps, and the rests in unit of meV:  $T = 0.078$ ,  $\Gamma = 0.1$  and  $W = 5$ .

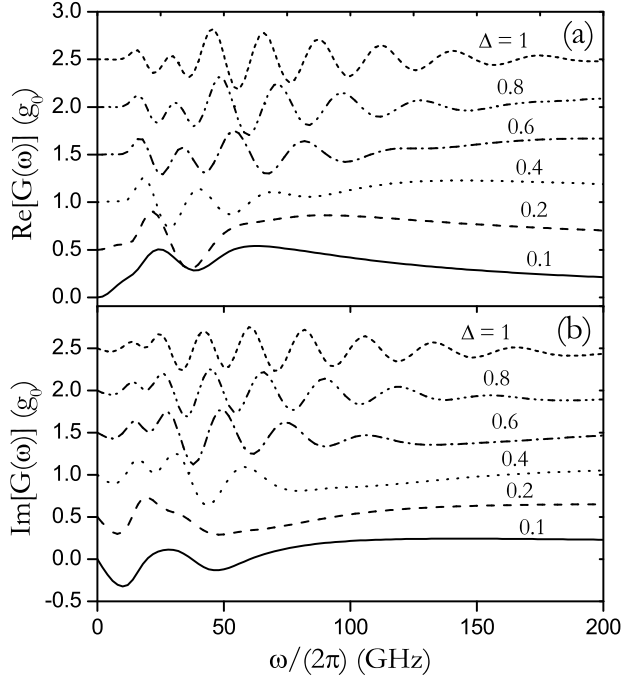


FIG. 9: (a) Real and (b) imaginary parts of  $G(\omega)$  under Gaussian voltages of different amplitudes. For both (a) and (b), the lines represent different  $\Delta$  in unit of meV. Same parameters are adopted as in Fig. 8. In both panels the lines are separated vertically by  $0.5 g_0$  for clarity.

function voltage, the lead level shift is  $\Delta(t) = \Delta\Theta(t)$ . With a tiny  $\Delta$ , the linear-response admittance as well as the associated charge relaxation resistance  $R_q$  should be reproduced from the above derivations for  $I(\omega)$ .<sup>23</sup>

The transient currents calculated by the HEOM approach are plotted in Fig. 10. It is shown that with a narrower lead conduction band, the initial overshooting of  $I(t)$  becomes less prominent and it takes longer time for the open system to reach the steady state. High-frequency oscillations are clearly observed for  $I(t)$  at the time  $0 \leq t \leq 25$  ps, which are due to the large amplitude

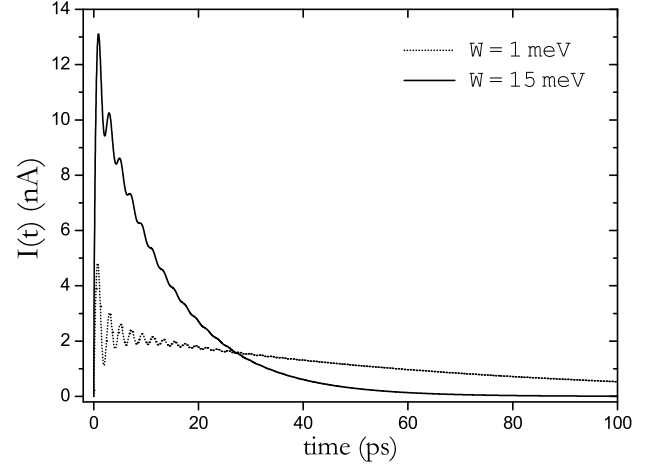


FIG. 10: Transient current responses to a step function voltage. The lines represent different bandwidths. Other parameters (in unit of meV):  $\Delta = 5$ ,  $T = 0.02$ ,  $\Gamma = 0.05$  and  $\epsilon_0 = 3$ .

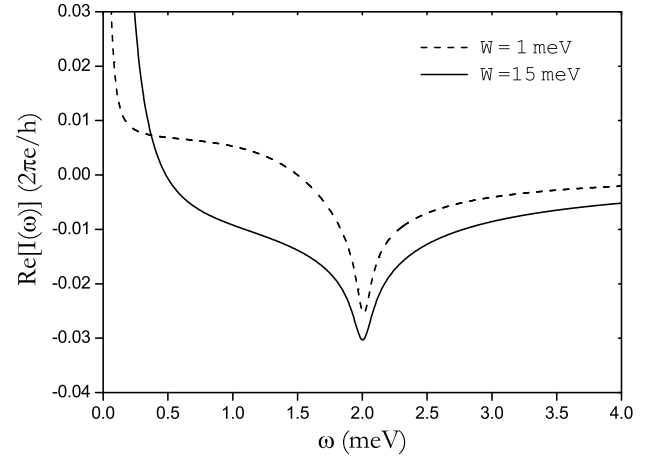


FIG. 11: The real part of  $I(\omega)$ . The inset magnifies the lines around the valleys. Results with finite  $W$  correspond to  $I(t)$  in Fig. 10. The other parameters are (in unit of meV):  $\Delta = 5$ ,  $\Gamma = 0.05$  and  $\epsilon_0 = 3$ .

of applied voltage. This nonlinear effect is confirmed by making a comparison to Fig. 1(a), where the rapid oscillation is absent from the transient current due to the much smaller  $\Delta$ . It is revealed from the Fourier analysis that the characteristic oscillation frequency is centered at  $\omega_0 = \Delta - \epsilon_0$ , as depicted in Fig. 11. In Fig. 12 we further investigate  $I(\omega)$  by plotting its dependence on  $\epsilon_0$  under a fixed  $\Delta$ . For all cases  $I(\omega)$  either reaches an extreme point or undergoes a sudden change in terms of its value at  $\omega = \omega_0$ . It is interesting to note that for  $\epsilon_0 < \mu$  the plotted  $\text{Re}[I(\omega)]$  exhibits a peak at  $\omega = \omega_0$ , while for  $\epsilon_0 > \mu$  a dip shows up. As  $\epsilon_0$  is drawn closer to  $\mu$ , the current response at the frequency  $\omega_0$  is more accentuated. In the time domain, this implies an enhanced oscillation amplitude for the transient current. For the resonant case, *i.e.*,  $\epsilon_0 = \mu$ , the function form of  $\text{Re}[I(\omega)]$  near  $\omega_0$  is  $\ln(x^2 + 1)/x$  with  $x = 2(\omega - \omega_0)/\Gamma$ , which is different from the typical Fano line shape  $(x + q)^2/(x^2 + 1)$ .<sup>24</sup>

The thermal influence on the transient current is also explored. In Fig. 13 we plot  $\text{Re}[I(\omega_0)]$  as a function of

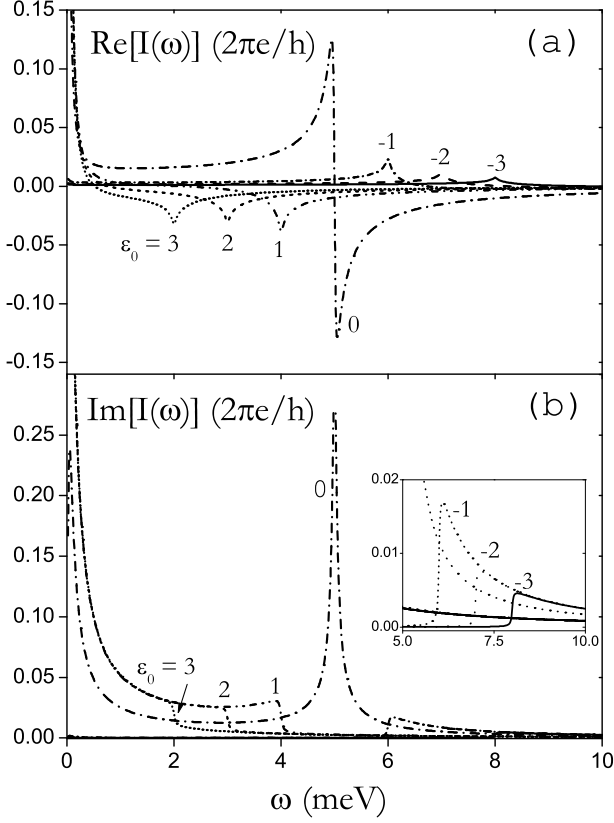


FIG. 12: (a) Real and (b) imaginary parts of  $I(\omega)$  under a step function voltage of  $\Delta = 5$  meV. The lines represent different  $\epsilon_0$  in unit of meV. The inset magnifies the down-right corner of panel (b). The other parameters are (in unit of meV):  $T = 0$ ,  $W = \infty$  and  $\Gamma = 0.05$ .

temperature. It is found that the system under investigation starts to respond sensitively to the environmental temperature at  $T \sim 0.01$  meV. Upon further increase of  $T$ , the thermal effect overwhelms the system–bath–coupling–induced linewidth, which is 0.05 meV in this specific case, and thus dominates the electronic dynamics of the reduced system.

### C. Transient current driven by a delta function voltage and its spectrum analysis

A delta function external field has been used to study the transient electronic dynamics of an isolated molecular system.<sup>25</sup> For an open system, such as the single-level QD system of our primary interest, a delta function applied voltage is also useful to investigate its dynamic properties. The time-dependent level shift considered is  $\Delta(t) = \Delta\Theta(t)\delta(t)$ . The advantage of such a delta function voltage is two-fold: (1) its Fourier transform  $\Delta(\omega) = \Delta/2$  is a constant, thus the current response of any frequency can be detected, with  $I(\omega) \propto G(\omega)$ ; (2) the HEOM (12) becomes a set of time-independent linear equations at  $t \geq 0^+$ , and an efficient Chebyshev propagator can be employed to solve the evolution of  $\rho_n(t)$ ,<sup>25,26</sup> which greatly reduces the computational cost.

To simulate the transient current in response to a delta

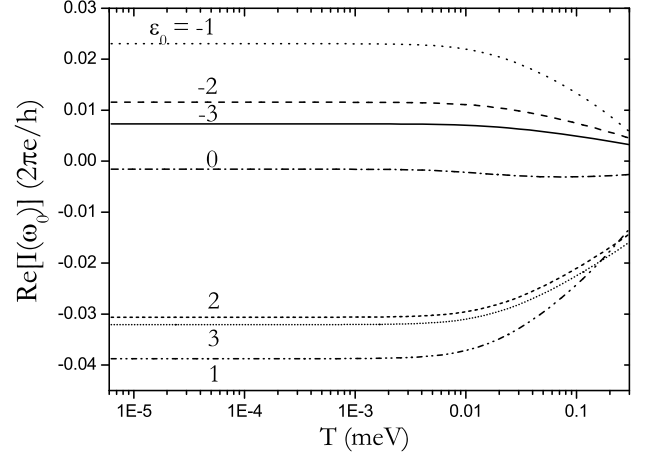


FIG. 13:  $\text{Re}[I(\omega_0)]$  as a function of temperature. The lines represent different values of  $\epsilon_0$  in unit of meV. The horizontal axis is in  $\log_{10}$  scale. Other parameters are:  $W = \infty$  and  $\Gamma = 0.05$  meV.

function voltage by the HEOM approach, we notice that  $\Delta(t)$  takes effect only within the infinitesimal interval, *i.e.*,  $t \in (0, 0^+)$ . Therefore, the reduced dynamics at  $(t > 0^+)$  can be solved by normal propagation of Eq. (12) (in absence of bias voltages) with the initial condition adjusted to  $\rho_n(0^+)$ . Consider a moderate amplitude  $\Delta$ , so that all the ADOs remain finite within  $t \in (0, 0^+)$ . Therefore, neither  $\rho_n^{\{+\}}$  nor  $\rho_n^{\{-}$  contributes as Eq. (12) is formally integrated from time  $t = 0$  to  $0^+$ :

$$\begin{aligned} \rho_n(0^+) &= \rho_n(0) + i \sum_n \sigma_n \int_0^{0^+} \Delta(\tau) \rho_n(\tau) d\tau \\ &= \frac{1}{1 - i\tilde{\Delta}_n} \rho_n(0). \end{aligned} \quad (17)$$

Here  $\rho_n(0)$  are the equilibrium reduced density matrix and associated ADOs, and  $\tilde{\Delta}_n$  is expressed as follows,

$$\tilde{\Delta}_n \equiv \sum_n \sigma_n \int_0^{0^+} \Delta(\tau) d\tau = \frac{\Delta}{2} \sum_n \sigma_n. \quad (18)$$

Due to the fact that  $\tilde{\Delta}_n|_{\tilde{n}=0} = 0$  we have  $\rho(0^+) = \rho(0)$ , *i.e.*, the reduced density matrix remains continuous upon the delta function perturbation.

In Fig. 14 we plot the calculated transient currents corresponding to different bandwidths. In both cases the current is instantaneously switched on to its maximal value at  $t = 0^+$ , and then relaxes back to zero. The peak value  $I_{\max} = I(0^+)$  is 21.4 nA for  $W = 15$  meV, and 11.5 nA for  $W = 1$  meV, respectively. The corresponding current spectrums are depicted in Fig. 15. The similarity in lineshape between Fig. 3 and Fig. 11 is noted, although the former is a linear response result while the latter belongs to the nonlinear regime. This is actually due to the factorization property of  $I(\omega)$  for the resonant tunneling case,<sup>23</sup> where the current spectrum can be expressed as  $I(\omega) = \sin(\Delta/2)X(\omega)$  in the resonant case ( $\epsilon_0 = \mu = 0$ ), where  $X(\omega)$  is some complex function independent of  $\Delta$ .



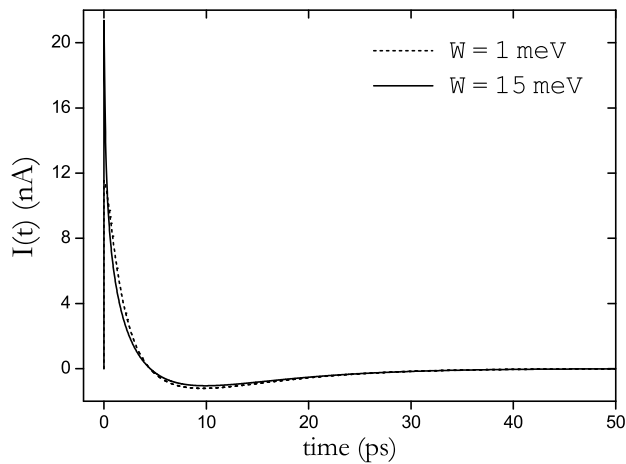


FIG. 14: Transient current responses to a delta function voltage. The lines represent different bandwidths. Other parameters are (in unit of meV):  $\Delta = 1$ ,  $T = 0.052$ ,  $\Gamma = 0.1$  and  $\epsilon_0 = 0$ .

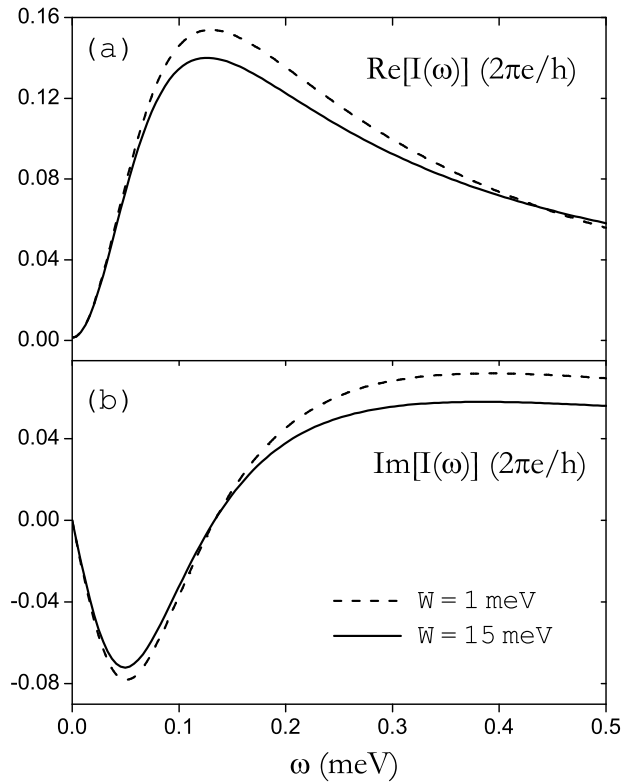


FIG. 15: (a) Real and (b) imaginary parts of  $I(\omega)$  under a delta function voltage. Results with finite  $W$  correspond to  $I(t)$  in Fig. 14. The common parameters are (in unit of meV):  $\Delta = 1$ ,  $\Gamma = 0.1$  and  $\epsilon_0 = 0$ .

## V. CONCLUSIONS AND COMMENTS

To conclude, we investigate the quantum coherent electronic dynamics of a single-level noninteracting QD coupled to one electrode. Simulations are carried out based on the HEOM formalism of QDT.<sup>13</sup> In the linear response regime, quantitatively accurate frequency-dependent admittance is obtained by the calculated transient current

response to an asymmetric Gaussian voltage pulse, for both resonant and off-resonant tunneling cases. It is verified that at a finite temperature, the dynamic admittance of the open QD system in the low frequency range can still be characterized by a classical  $RLC$  circuit. However, the charge relaxation resistance  $R_q$  is found deviated from half a resistance quantum, but depends on both the temperature and the system-bath coupling strength. The concept of the equivalent classical circuit breaks down under higher bias. Complicated nonlinear features are observed, such as the activation of high-frequency current components with an increasing voltage amplitude. Transient current responses to step and delta function voltages are also explored. The basic features of the associated electronic dynamics are analyzed and discussed. The analytical and numerical results obtained in Sec. III and IV serve as convenient basis to understand the electronic dynamics of an interacting open system, in which the HEOM formalism is in principle exact. Work along this direction is underway.

The HEOM approach also has great implications for time-dependent quantum transport in nanoscopic molecular devices. Formalisms based on NEGF method,<sup>27,28,29,30,31,32,33,34,35,36,37,38,39</sup> Floquet theory,<sup>40,41,42,43,44,45</sup> and QDT<sup>46,47,48,49</sup> have been proposed. First-principles calculations have been carried out on realistic electronic devices.<sup>22</sup> However, in these simulations, approximate schemes for the dissipative dynamics in real time are inevitably introduced. For instance, the complete second-order formulation<sup>18,50,51</sup> and the WBL approximation were adopted to simulate the steady and transient current through a molecular device with time-dependent density-functional theory.<sup>22</sup> It is thus important that these approximate schemes can be improved systematically. Since the QDT-HEOM approach is capable of yielding exact results for quantum dissipative dynamics, it can be utilized to calibrate the approximated methodologies, and we also expect it to provide some guidelines for the potential progress of the approximate formalisms.

## Acknowledgments

Support from the RGC (604007 and 604508) of Hong Kong is acknowledged.

## APPENDIX: NUMERICAL VALIDATION

We verify our numerical implementation of HEOM formalism by comparisons to known exact quantum transport results achievable via other methods. Three cases of noninteracting QDs coupled to left and right electrodes ( $L$  and  $R$ ) of Lorentzian spectral density functions are demonstrated as follows.

The first case studies the time-dependent transport through a single-level spinless QD driven by a step-function voltage pulse, calculated before exactly by the NEGF method.<sup>21,52,53</sup> In Fig. 16 we plot the transient currents calculated via the HEOM approach on the same system as that of Fig. 2 in Ref. 21. Our results agree

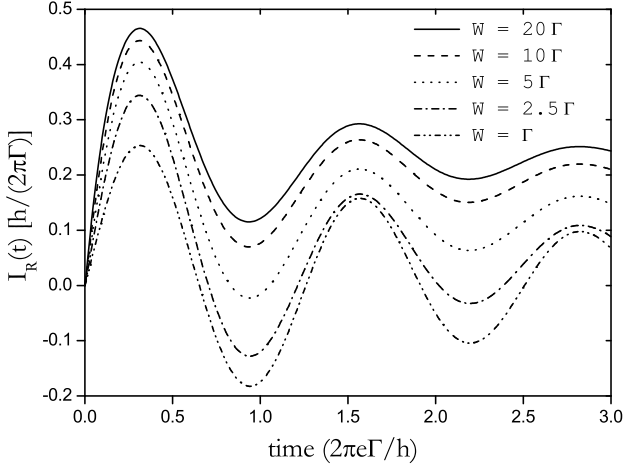


FIG. 16: Transient current through R-lead,  $I_R(t)$ , in response to a step-function voltage pulse applied on R-lead. The lines correspond to different lead bandwidths. Other parameters:  $\Gamma_L = \Gamma_R = 0.5\Gamma$ ,  $T = 0.1\Gamma$ ,  $W_L = W_R = W$  and  $\Delta = 10\Gamma$ . This figure reproduces Fig. 2 in Ref. 21.

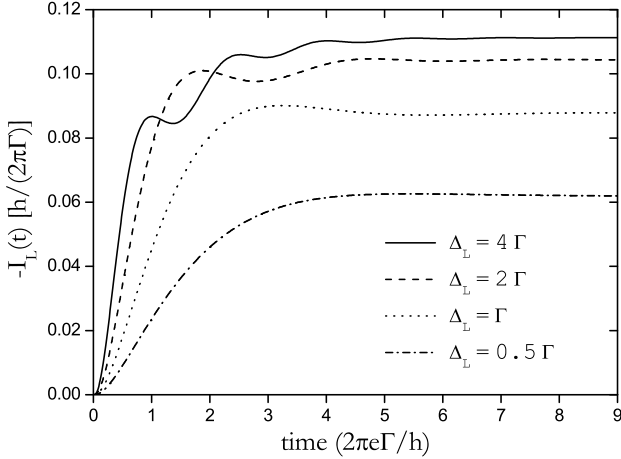


FIG. 17: Transient currents through L-lead,  $I_L(t)$ , in response to a step-function voltage pulse applied on R-lead. The lines correspond to different voltage amplitudes. Other parameters:  $\Gamma_L = \Gamma_R = 0.5\Gamma$ ,  $T = 0.05\Gamma$  and  $W_L = W_R = 20\Gamma$ . This figure reproduces Fig. 1 in Ref. 52.

quantitatively. The QD is initially in equilibrium with zero bias. External voltage pulses are switched on from the time  $t = 0$ , which results in current flows through the leads  $L$  and  $R$  at  $t > 0$ . Hereafter we denote  $\Delta_L(t)$  and  $\Delta_R(t)$  as the time-dependent energy shifts for the lead  $L$  and  $R$  due to the applied voltages  $V_L(t)$  and  $V_R(t)$ , respectively, *i.e.*,  $\Delta_\alpha(t) = -eV_\alpha(t)$ . For simulations presented in this section, we set  $\Delta_L(t) = 0$  for all  $t$ , and  $\Delta_R(t) = \Delta\Theta(t)$ , where  $\Theta(t)$  is a step function turned on at  $t = 0$ , and  $\Delta$  is a constant amplitude. The system level energy is time-dependent as  $\tilde{\epsilon}_0(t) = \epsilon_0 + \Delta_D(t)$  with  $\Delta_D(t) = [\Delta_L(t) + \Delta_R(t)]/2$ .

The second example is similar to the first one, but with  $\Delta_D(t) = 0$ . The calculated transient currents displayed in Fig. 17 accurately reproduce previous simulations (*cf.* Fig. 1 in Ref. 52) by the NEGF method with all the non-Markovian features preserved.<sup>52,53</sup>

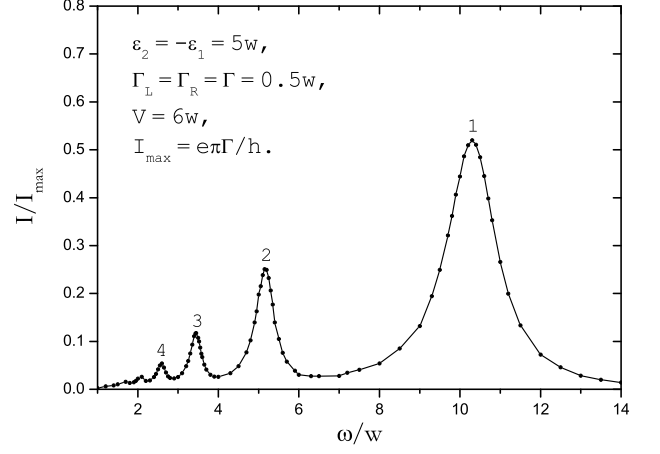


FIG. 18: Time-averaged current  $I$  (in unit of  $I_{\max} = e\Gamma/2h$ ) through a noninteracting double QD, driven by *ac* gate voltage (see Ref. 40 for details). The interdot coupling strength  $w = 0.1$  meV. Other parameters:  $\mu_L^{\text{eq}} = \mu_R^{\text{eq}} = 0$ ,  $T = w$  and  $W_L = W_R = 20w$ . The characteristic multiphoton-assisted resonance energies  $\omega_N = \frac{1}{N}\sqrt{(\epsilon_2 - \epsilon_1)^2 + 4w^2}$  are labeled by numbers  $N = 1 \sim 4$ . This figure reproduces Fig. 3 in Ref. 40.

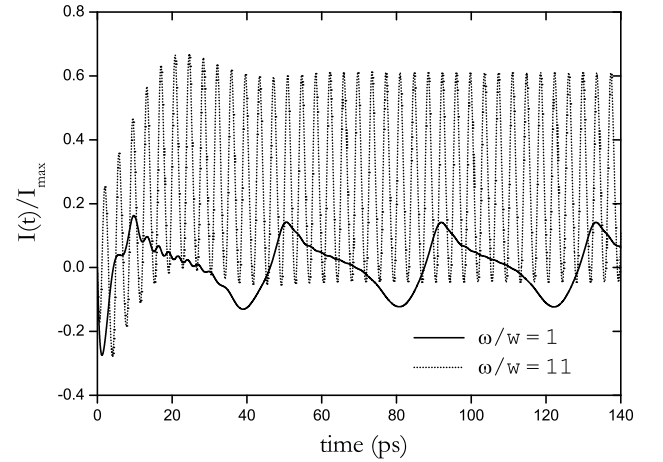


FIG. 19: Transient current  $I_L(t)$  (in unit of  $I_{\max} = e\Gamma/2h$ ) through a noninteracting double QD. The system setup and other parameters are same as in Fig. 18.

The third example investigates the resonant photon-assisted tunneling through QDs where results have been obtained by a combined method of NEGF and Floquet formalisms.<sup>40,44</sup> In Ref. 40, nonequilibrium electron pumping through a double QD system driven by *ac* gate voltage was simulated. Multi-photon-assisted tunneling was resolved in time-average current spectrum. Since the HEOM approach admits an arbitrary time-dependent external field, a sinusoidal gate voltage can be treated readily. However, instead of the frequency-domain calculation conducted in Ref. 40, with our present coding scheme we need to propagate Eq. (12) in real time for every individual frequency. This makes the simulation for the entire current spectrum rather tedious. Nonetheless, to further justify our numerical procedures, we have managed to carry out such a simulation and compared to reported results. A noninteracting double QD system coupled to two leads is studied. The time-averaged

current is evaluated as the system reaches a quasi-steady state for each gate voltage frequency  $\omega$ . We take the same parameter set as adopted by Fig. 3 in Ref. 40, and the HEOM calculation result is plotted in Fig. 18. The quantitative agreement between our Fig. 18 and result shown in Ref. 40 is noted. In particular, the characteristic  $N$ -photon-assisted resonance frequencies are correctly reproduced, as demonstrated in Fig. 18. This test again validates our numerical procedures. It is worth mention-

ing that the Floquet formalism treats the quasi-steady dynamics driven by an *ac* external field, while our HEOM formalism allows access to much broader information beyond this, such as the establishment of a quasi-steady state in real time. For instance, Fig. 19(a) and (b) depict the time evolution of a double QD driven by an *ac* gate voltage switched on from  $t = 0$  for  $\omega/w = 0.1$  and 1.1, respectively, where  $w$  is the inter-dot coupling strength as the system setup is the same as in Fig. 18.

- 
- \* Electronic address: chxzheng@ust.hk; yyan@ust.hk
- <sup>1</sup> M. Büttiker, H. Thomas, and A. Prêtre, *Phys. Lett. A* **180**, 364 (1993).
  - <sup>2</sup> M. Büttiker, A. Prêtre, and H. Thomas, *Phys. Rev. Lett.* **70**, 4114 (1993).
  - <sup>3</sup> A. Prêtre, H. Thomas, and M. Büttiker, *Phys. Rev. B* **54**, 8130 (1996).
  - <sup>4</sup> S. E. Nigg, R. López, and M. Büttiker, *Phys. Rev. Lett.* **97**, 206804 (2006).
  - <sup>5</sup> J. Wang, B. Wang, and H. Guo, *Phys. Rev. B* **75**, 155336 (2007).
  - <sup>6</sup> M. P. Anantram and S. Datta, *Phys. Rev. B* **51**, 7632 (1995).
  - <sup>7</sup> J. Gabelli, G. Fève, J.-M. Berroir, B. Placais, A. Cavanna, B. Etienne, Y. Jin, and D. C. Glattli, *Science* **313**, 499 (2006).
  - <sup>8</sup> J. M. Gerling, D. A. Crim, D. G. Morgan, P. D. Coleman, W. Kopp, and H. Morkoc, *J. Appl. Phys.* **61**, 271 (1987).
  - <sup>9</sup> E. R. Brown, C. D. Parker, and T. C. L. G. Sollner, *Appl. Phys. Lett.* **54**, 934 (1989).
  - <sup>10</sup> H. C. Liu, *J. Appl. Phys.* **69**, 2705 (1991).
  - <sup>11</sup> Y. Fu and S. C. Dudley, *Phys. Rev. Lett.* **70**, 65 (1993).
  - <sup>12</sup> J. S. Jin et al., *J. Chem. Phys.* **126**, 134113 (2007).
  - <sup>13</sup> J. S. Jin, X. Zheng, and Y. J. Yan, *J. Chem. Phys.* **128**, 234703 (2008).
  - <sup>14</sup> R. X. Xu, P. Cui, X. Q. Li, Y. Mo, and Y. J. Yan, *J. Chem. Phys.* **122**, 041103 (2005).
  - <sup>15</sup> R. X. Xu and Y. J. Yan, *Phys. Rev. E* **75**, 031107 (2007).
  - <sup>16</sup> Y. Tanimura, *Phys. Rev. A* **41**, 6676 (1990).
  - <sup>17</sup> C. Meier and D. J. Tannor, *J. Chem. Phys.* **111**, 3365 (1999).
  - <sup>18</sup> Y. J. Yan and R. X. Xu, *Annu. Rev. Phys. Chem.* **56**, 187 (2005).
  - <sup>19</sup> R. P. Feynman and F. L. Vernon, Jr., *Ann. Phys. (N. Y.)* **24**, 118 (1963).
  - <sup>20</sup> W. H. Press, S. A. Teukolsky, W. T. Vetterling, and B. P. Flannery, *Numerical Recipes in Fortran*, Cambridge University Press, New York, 1992.
  - <sup>21</sup> J. Maciejko, J. Wang, and H. Guo, *Phys. Rev. B* **74**, 085324 (2006).
  - <sup>22</sup> X. Zheng, F. Wang, C. Y. Yam, Y. Mo, and G. H. Chen, *Phys. Rev. B* **75**, 195127 (2007).
  - <sup>23</sup> Y. Mo, G. H. Chen, X. Zheng, and Y. J. Yan, (in preparation).
  - <sup>24</sup> U. Fano, *Phys. Rev.* **124**, 1866 (1961).
  - <sup>25</sup> F. Wang, C.-Y. Yam, G. H. Chen, and K. N. Fan, *J. Chem. Phys.* **126**, 134104 (2007).
  - <sup>26</sup> R. Baer and D. Neuhauser, *J. Chem. Phys.* **121**, 9803 (2004).
  - <sup>27</sup> L. Y. Chen and C. S. Ting, *Phys. Rev. Lett.* **64**, 3159 (1990).
  - <sup>28</sup> D. C. Langreth and P. Nordlander, *Phys. Rev. B* **43**, 2541 (1991).
  - <sup>29</sup> V. V. Afonin and A. M. Rudin, *Phys. Rev. B* **49**, 10466 (1994).
  - <sup>30</sup> A.-P. Jauho, N. S. Wingreen, and Y. Meir, *Phys. Rev. B* **50**, 5528 (1994).
  - <sup>31</sup> R. López, R. Aguado, G. Platero, and C. Tejedor, *Phys. Rev. B* **64**, 075319 (2001).
  - <sup>32</sup> I. Knezevic and D. K. Ferry, *Phys. Rev. E* **67**, 066122 (2003).
  - <sup>33</sup> Y. Zhu, J. Maciejko, T. Ji, H. Guo, and J. Wang, *Phys. Rev. B* **71**, 075317 (2005).
  - <sup>34</sup> S. Kurth, G. Stefanucci, C. O. Almbladh, A. Rubio, and E. K. U. Gross, *Phys. Rev. B* **72**, 035308 (2005).
  - <sup>35</sup> X. Qian, J. Li, X. Lin, and S. Yip, *Phys. Rev. B* **73**, 035408 (2006).
  - <sup>36</sup> V. Moldoveanu, V. Gudmundsson, and A. Manolescu, *Phys. Rev. B* **76**, 165308 (2007).
  - <sup>37</sup> V. Moldoveanu, V. Gudmundsson, and A. Manolescu, *Phys. Rev. B* **76**, 085330 (2007).
  - <sup>38</sup> F. M. Souza, S. A. Leão, R. M. Gester, and A. P. Jauho, *Phys. Rev. B* **76**, 125318 (2007).
  - <sup>39</sup> S. Weiss, J. Eckel, M. Thorwart, and R. Egger, *Phys. Rev. B* **77**, 195316 (2008).
  - <sup>40</sup> C. A. Stafford and N. S. Wingreen, *Phys. Rev. Lett.* **76**, 1916 (1996).
  - <sup>41</sup> A. Tikhonov, R. D. Coalson, and Y. Dahnovsky, *J. Chem. Phys.* **116**, 10909 (2002).
  - <sup>42</sup> C. E. Creffield and G. Platero, *Phys. Rev. B* **65**, 113304 (2002).
  - <sup>43</sup> C. E. Creffield and G. Platero, *Phys. Rev. B* **66**, 235303 (2002).
  - <sup>44</sup> G. Platero and R. Aguado, *Phys. Rep.* **395**, 1 (2004).
  - <sup>45</sup> T. Brandes, R. Aguado, and G. Platero, *Phys. Rev. B* **69**, 205326 (2004).
  - <sup>46</sup> P. Cui, X. Q. Li, J. S. Shao, and Y. J. Yan, *Phys. Lett. A* **357**, 449 (2006).
  - <sup>47</sup> X. Q. Li and Y. J. Yan, *Phys. Rev. B* **75**, 075114 (2007).
  - <sup>48</sup> S. Welack, M. Schreiber, and U. Kleinekathöfer, *J. Chem. Phys.* **124**, 044712 (2006).
  - <sup>49</sup> J. Villavicencio, I. Maldonado, R. Sánchez, E. Cota, and G. Platero, *Appl. Phys. Lett.* **92**, 192102 (2008).
  - <sup>50</sup> Y. J. Yan, *Phys. Rev. A* **58**, 2721 (1998).
  - <sup>51</sup> R. X. Xu and Y. J. Yan, *J. Chem. Phys.* **116**, 9196 (2002).
  - <sup>52</sup> J. N. Pedersen and A. Wacker, *Phys. Rev. B* **72**, 195330 (2005).
  - <sup>53</sup> G. Stefanucci and C.-O. Almbladh, *Phys. Rev. B* **69**, 195318 (2004).